Journal of the Ceramic Society of Japan 121 [8] 583-588 2013 Paper

Characterization of $BaTiO_3$ crystals formed in aluminosilicate glasses and their laser patterning

Takayuki KOMATSU,† Takashi OIKAWA and Tsuyoshi HONMA

Department of Materials Science and Technology, Nagaoka University of Technology, 1603–1 Kamitomioka-cho, Nagaoka, Niigata 940–2188, Japan

$BaTiO_3$ crystals synthesized through the crystallization of $40BaO–40TiO_2–15SiO_2–5Al_2O_3$ glass were characterized from Raman scattering spectrum, second harmonic generation (SHG), and polarization measurements. The structure of $BaTiO_3$ nanocrystals (∼70 nm) formed initially was suggested to be pseudo-cubic (small tetragonality), and perovskite-type ferroelectric $BaTiO_3$ crystals were formed in the heat-treatments at high temperatures of ∼930°C. The lines consisting of $BaTiO_3$ crystals were patterned at the surface of CuO-doped glass by irradiations of continuous-wave Yb:YVO_4 lasers with a wavelength of 1080 nm. It was confirmed that $BaTiO_3$ being present in the laser-irradiated parts exhibits SHGs and, in particular, $BaTiO_3$ formed in the laser ablation region has a tetragonal structure and a Curie temperature of ∼135°C.

Key-words : $BaTiO_3$, Glass, Crystallization, Raman scattering spectrum, Second harmonic generation, Laser pattering

[Received March 1, 2013; Accepted April 12, 2013]

1. Introduction

Functional materials have been synthesized through various methods. Crystallization of glass is a unique method for the fabrication of transparent and dense condensed materials with desired shapes, nanostructures, and highly oriented crystals, and a crystallization technique has been applied to various glass systems in order to design active functional crystals with high performances such as second harmonic generation (SHG) or ferroelectricity. Barium titanate, $BaTiO_3$, exhibits various excellent optical and dielectric properties and is one of the most important inorganic materials which have been used practically in various electronic devices. It is, therefore, of interest and of importance to design crystallized glasses (glass-ceramics) consisting of perovskite-type ferroelectric $BaTiO_3$ crystals. Indeed, so far, several researchers have tried to fabricate crystallized glasses containing $BaTiO_3$ or $Ba_{1-x}Sr_xTiO_3$ crystals,[1)–18)] as summarized in **Table 1**, and for instance, Borrelli and Layton[5)] observed a large electrooptic effect (EO) in transparent crystallized glasses with $BaTiO_3$ crystals.

Usually, crystallized glasses are fabricated by heat treatment of precursor glasses in an electric furnace, and the size, amount, and morphology of target crystals are designed by controlling heat treatment conditions (i.e., nucleation and crystal growth rates) and glass composition. In particular, in the case of $BaTiO_3$, it is impossible to fabricate bulk glasses using normal melt-quenching speeds in the binary $BaO–TiO_2$ system, and thus glass-forming oxides such as SiO_2 and B_2O_3 are required to be added, e.g., $BaO–TiO_2–SiO_2$, as shown in Table 1. Laser-induced crystallization in glass has also received much attention, because in which active crystals are patterned only in spatially selected parts.[19)–22)] Patterning of active crystals in glasses will have a high potential for practical applications in various active devices. It is of interest to pattern $BaTiO_3$ crystals in glasses by using a laser-induced crystallization technique. Yonesaki et al.[13)] tried to irradiate femtosecond (∼120 fs) pulsed Ti: sapphire laser (wavelength: $\lambda = 800$ nm) to $Na_2O–BaO–TiO_2–SiO_2$ glasses and confirmed the formation of $BaTiO_3$ together with $Ba_2TiSi_2O_8$ crystals. The structure (i.e., cubic or tetragonal) of $BaTiO_3$ formed, however, has not been determined in their report.[13)]

The purpose of this study is to characterize $BaTiO_3$ crystals synthesized through the crystallization of $BaO–TiO_2–SiO_2–Al_2O_3$ glasses and to pattern crystal lines consisting of perovskite-type (tetragonal) $BaTiO_3$ at the glass surface by using laser irradiations. In the present study, a laser-induced crystallization technique called transition metal atom heat processing (TMAH) was applied,[19)–23)] in which continuous-wave (cw) Yb:YVO_4 lasers with $\lambda = 1080$ nm have been used. Using the TMAH technique, for instance, the present authors' group has succeeded in patterning ferroelectric $LiNbO_3$ crystal lines with high orientations.[24)–27)] The study on the laser patterning of $BaTiO_3$ crystal lines in glasses has not been, however, reported so far.

2. Experimental procedures

Glasses with the compositions of $40BaO–40TiO_2–15SiO_2–5Al_2O_3$ (mol%) and $1CuO–40BaO–40TiO_2–15SiO_2–5Al_2O_3$ (mol) were prepared using a conventional melt-quenching technique. Commercial powders of raw materials of $BaCO_3$, TiO_2, SiO_2, Al_2O_3, and CuO were mixed and melted in a platinum crucible at 1400°C for 1 h in air in an electric furnace. The melts were poured onto an iron plate and pressed to a thickness of ∼1.5 mm with another iron plate. The glass transition, T_g, and crystallization peak, T_p, temperatures were determined using differential thermal analyses (DTA) at a heating rate of 10 K/min. The optical absorption spectrum for the CuO-doped sample was measured in the wavelength range of 250–2000 nm using a spectrometer (Shimadzu U-3120).

The crystalline phases formed by heat treatments were examined from X-ray diffraction (XRD) analyses (Cu Kα radiation) at room temperature and micro-Raman scattering spectrum measurements (Tokyo Instruments Co., Nanofinder; Ar^+ laser 488

† Corresponding author: T. Komatsu; E-mail: komatsu@mst.nagaokaut.ac.jp

DOI http://dx.doi.org/10.2109/jcersj2.121.583

Table 1. Glass composition and features for the crystallization of $BaTiO_3$ and $(Sr,Ba)TiO_3$ in glasses reported so far[1)–18)]

Glass composition (mol%)	Features	Ref.
xBaTiO$_3$–(100-x)BaAl$_2$Si$_2$O$_8$	Dielectric constant of 1200	1)
(100-x-y)BaTiO$_3$–xSiO$_2$–yAl$_2$O$_3$, $x = 10$–60, $y = 0$–20	Lamellar shape	2),3)
BaTiO$_3$–SiO$_2$–Al$_2$O$_3$	Low network former content	4)
BaTiO$_3$–SiO$_2$	Electro-optic effect	5)
BaO–TiO$_2$–B$_2$O$_3$	Glass formation, Crystalline phases	6)
15BaO–15TiO$_2$–70TeO$_2$	Transparent, TeO$_2$ glass former	7)
50BaO–20TiO$_2$–30B$_2$O$_3$	Twin-roller quenching	8)
40BaO–30TiO$_2$–20SiO$_2$–7Al$_2$O$_3$–3AlF$_3$	Direct crystallization	9)
42.9BaO–35.8TiO$_2$–14.3SiO$_2$–7.2Al$_2$O$_3$	Size effect on dielectric property	10),11)
15BaO–15TiO$_2$–70TeO$_2$	SHG, $d_{15} = 0.31$ pm/V	12)
5Na2O–36BaO–39TiO$_2$–20SiO$_2$	Femtosecond (120 fs) laser, dot	13)
60BaTiO$_3$–40Li$_2$B$_4$O$_7$	BaTiO$_3$, Li$_2$B$_4$O$_7$, Ba(BO$_3$)$_2$	14)
60(Ba$_{1-x}$Sr$_x$)TiO$_3$–25SiO$_2$–15AlF$_3$	Ferroelectric Ba$_{1-x}$Sr$_x$TiO$_3$	15)
90(Ba$_{0.7}$Sr$_{0.3}$)TiO$_3$–10(B$_2$O$_3$–xSiO$_2$)	Kinetics, $E_a = 705$ kJ/mol	16)
70(Ba$_{0.7}$Sr$_{0.3}$)TiO$_3$–30(Al$_2$O$_3$–SiO$_2$)	Kinetics, $E_a = 432$ kJ/mol	17)
Ba$_{0.6}$Sr$_{0.4}$TiO$_3$–SiO$_2$–B$_2$O$_3$–K$_2$O–La$_2$O$_3$	Kinetics, $E_a = 762$ kJ/mol	18)

nm). SHGs of heat-treated samples were measured by using a Maker fringe technique with Q-switch Nd:YAG laser ($\lambda =$ 1064 nm). The CuO-doped sample was mechanically polished to mirror finish with CeO_2 powders, and cw Yb:YVO_4 fiber lasers with $\lambda = 1080$ nm were irradiated onto the surface of the glass using objective lens (50 times magnification). The sample was put on the stage and mechanically moved during laser irradiations to construct crystal lines. The morphology and crystalline phase of lines were examined from polarized optical microscope (POM), confocal scanning laser microscope (CSLM) (Olympus-OLS 3000) observations, micro-Raman scattering spectrum, and SHG measurements.

3. Results and discussion

As shown in Table 1, several glass systems and compositions have been examined for the preparation of crystallized glasses with $BaTiO_3$ crystals, and it has been recognized that the system of BaO–TiO$_2$–SiO$_2$–Al$_2$O$_3$ is a good candidate.[2)–4),9)–11)] Kokubo et al.[2)] examined the glass-forming region and the crystallization of $BaTiO_3$ in the BaO–TiO$_2$–SiO$_2$–Al$_2$O$_3$ system and reported that the maximum content of BaO and TiO$_2$ is around 40 mol%. We examined the crystallization behavior of $BaTiO_3$ in several glasses with different compositions such as 40BaO–30TiO$_2$–20SiO$_2$–10Al$_2$O$_3$ and 35BaO–45TiO$_2$–15SiO$_2$–5Al$_2$O$_3$, and finally we selected a glass with the composition of 40BaO–40TiO$_2$–15SiO$_2$–5Al$_2$O$_3$ containing a large amount of BaO and TiO$_2$ in this study. In a previous study,[28)] we examined the laser-induced crystallization behavior of a glass with the composition of 40BaO–40TiO$_2$–20B$_2$O$_3$ and found that nonlinear optical Ba$_3$Ti$_3$O$_6$(BO$_3$)$_2$ crystals are patterned.

3.1 Usual crystallization in an electric furnace

Prior to the patterning of $BaTiO_3$ crystal lines by laser irradiations, the usual crystallization behavior in an electric furnace for 40BaO–40TiO$_2$–15SiO$_2$–5Al$_2$O$_3$ glass (designated here as BTSA glass), i.e., homogeneous and constant heating for a whole part of the glass, was examined, and the crystal structure and dielectric properties of $BaTiO_3$ crystals synthesized were characterized.

The melt-quenched BTSA sample prepared in this study maintained a good optical transparency, and any inhomogeneous microstructures such as large-scaled phase separations and partial crystallizations were not detected. The amorphous state in the melt-quenched sample was confirmed from the XRD pattern, in which only halo pattern was observed. The DTA patterns for the bulk and powder samples of the BTSA glass are shown in **Fig. 1**, indicating the presence of two exothermic peaks. They provide the values of $T_g = 683$°C, $T_{p1} = 826$°C, and $T_{p2} = 937$°C for the bulk sample and $T_g = 684$°C, $T_{p1} = 773$°C, and $T_{p2} = 960$°C for the powder sample. The difference in the values of T_{p1} and T_{p2} for bulk and powder samples suggests that the main crystallization mechanism in the BTSA glass would be surface crystallization. The large difference between T_g and T_{p1} in the bulk sample, i.e., $\Delta T = T_{p1} - T_g = 143$°C, indicates that the thermal stability against crystallization is relatively high. Usually, it has been recognized that glasses showing $\Delta T > 100$°C have high thermal stability and glasses showing $\Delta T \ll 100$°C tend to crystallize easily. For instance, 30MoO$_3$–50ZnO–20B$_2$O$_3$ glass has the value of $\Delta T = 40$°C and forms α-ZnMoO$_4$ crystals easily.[29)]

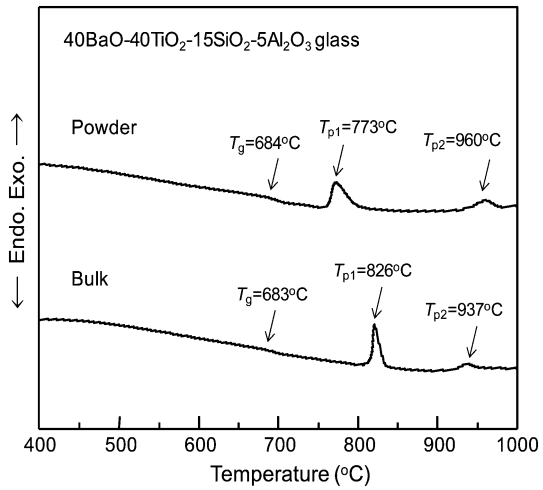

Fig. 1. DTA patterns for the bulk and powder samples of 40BaO–40TiO$_2$–15SiO$_2$–5Al$_2$O$_3$ glass. T_g and T_p are the glass transition and crystallization peak temperatures, respectively. The heating rate was 10 K/min.

The XRD patterns for the samples obtained by heat treatments at $T_{p1} = 826$°C for 5 h, $T_{p2} = 937$°C for 5 h, and $T = 1200$°C for 3 h are shown in **Fig. 2**. It is seen that $BaTiO_3$ crystals are formed in all heat-treated samples. In particular, all XRD peaks observed for the sample heat-treated at T_{p1} are assigned to the $BaTiO_3$ crystalline phase (the Joint Committee on Powder Diffraction

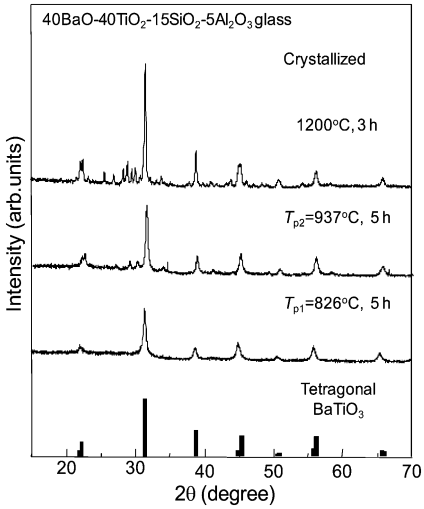

Fig. 2. XRD patterns for the heat-treated samples in $40BaO–40TiO_2–15SiO_2–5Al_2O_3$ glass. The XRD pattern for the tetragonal $BaTiO_3$ is taken from the JCPDS card (005–0626).

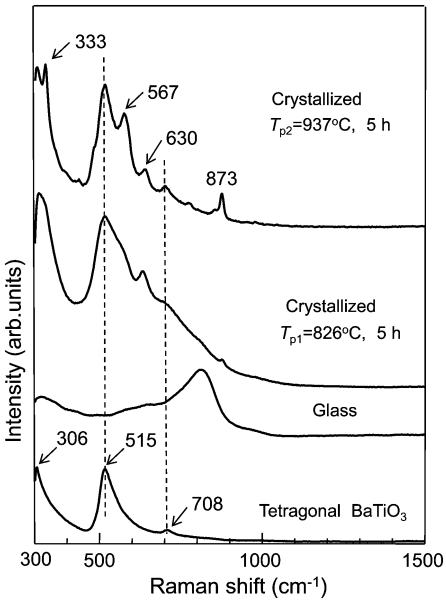

Fig. 3. Raman scattering spectra at room temperature for the heat-treated samples in $40BaO–40TiO_2–15SiO_2–5Al_2O_3$ glass.

Standards (JCPDS): 005–0626), demonstrating that the first exothermic peaks in the DTA pattern (Fig. 1) corresponds to the crystallization of $BaTiO_3$. The average particle size of $BaTiO_3$ crystals formed in this heat-treated ($T_{p1} = 826$°C for 5 h) sample was estimated from the peak width of XRD pattern by using Scherrer's equation, in which the peak corresponding to the (101) plane appeared at $2\theta \sim 31.6$ was used for the calculation. The value of ~70 nm was obtained, suggesting the formation of $BaTiO_3$ nanocrystals. In the samples heat-treated at T_{p2} and 1200°C, other crystalline phase (unidentified) is also formed.

The Raman scattering spectra at room temperature for the glass and heat-treated samples are shown in **Fig. 3** together with the data for tetragonal $BaTiO_3$ crystals (commercially available). Three Raman peaks observed at 306, 515, and 708 cm^{-1} in tetragonal $BaTiO_3$ (*P*4*mm*) are known to be characteristic for the tetragonal phase, i.e., the peaks at ~710, ~515, and ~305 cm^{-1}

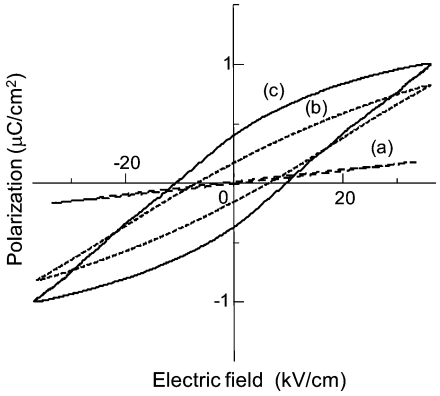

Fig. 4. Relationship between polarization and electric field for the heat-treated samples in $40BaO–40TiO_2–15SiO_2–5Al_2O_3$ glass. The curves of (a), (b), and (c) are for the sample heat-treated at T_{p1}(826°C), the sample heat-treated at T_{p2} (937°C), and the sample heat-treated at 1200°C, respectively.

are assigned to the Raman-active modes of $E(4LO) + A_1(3LO)$, $E(4TO) + A_1(3TO)$, and $E(3TO) + E(2LO)$, respectively.[30)–32)] In the glass, a broad peak being typical for glassy materials is observed at ~820 cm^{-1}. In the sample heat-treated at $T_{p1} =$ 826°C for 5 h, the peak having a strong intensity is observed at 515 cm^{-1}, and the other peak is detected at 630 cm^{-1}. It should be pointed out that a broad peak with a small intensity is also observed at ~708 cm^{-1} for this heat-treated ($T_{p1} = 826$°C) sample. Furthermore, the broad peak observed at ~820 cm^{-1} in the glass was almost disappeared in this heat-treated ($T_{p1} = 826$°C) sample. In the sample heat-treated at $T_{p2} = 937$°C, several peaks are observed at ~306, 333, 515, 567, 630, 708, and 873 cm^{-1}. It is, therefore, considered from Fig. 3 that at least tetragonal $BaTiO_3$ crystals are formed in the sample heat-treated at $T_{p2} =$ 937°C. At this moment, the peaks appeared at 333, 567, 630, and 873 cm^{-1} are not assigned, but would be due to the other crystalline phase (unidentified) (Fig. 2).

The relationship between polarization and electric field for the heat-treated samples are shown in **Fig. 4**. Clear hysteresis curves are observed for the samples heat-treated at T_{p2} and 1200°C. On the other hand, the sample heat-treated at T_{p1} does not exhibit any clear hysteresis. The second harmonic (SH) intensity, i.e., the Maker fringe patterns, for the base glass and heat-treated samples are shown in **Fig. 5**. For SH intensity measurements, the incident angle of linearly polarized lasers against the surface of samples (thickness: 0.2 mm) was 90°, and linearly polarized incident lasers are rotated against the surface of samples. The relation between incident lasers and samples is shown schematically in Fig. 5. It is found that the SH intensity increases with increasing heat treatments temperature. In particular, clear and strong SHGs were observed for the samples heat-treated at 1200°C. The results shown in Figs. 2 to 5 suggest that $BaTiO_3$ crystals present in the samples heat-treated at T_{p2} and 1200°C might be tetragonal, i.e., perovskite-type ferroelectric $BaTiO_3$. Furthermore, because any angular dependence in the Maker fringe patterns (Fig. 5) was not observed, $BaTiO_3$ crystals might be formed randomly without any distinct orientation. It is well known that a clear relationship exists between decreasing crystallite size (<1 μm) and decreasing tetragonality, leading to the phase transition from tetragonal to cubic for $BaTiO_3$ particles below a critical size.[30)] Suzuki and Kijima[33)] reported that $BaTiO_3$ nanoparticles under 30 nm are assigned to a perfect cubic structure, and in the range from 30 to 70 nm, the stable phase at room temperature transformed gradu-

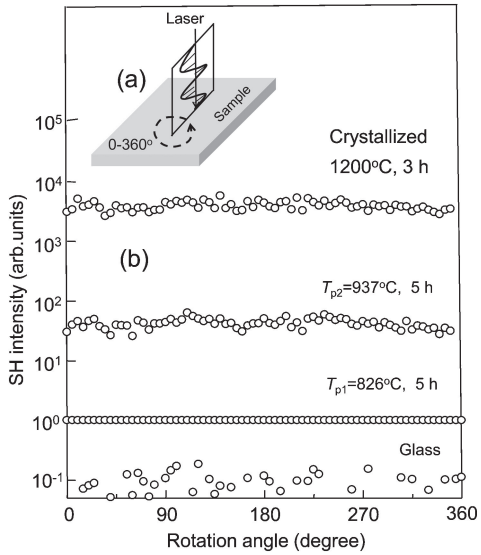

Fig. 5. Second harmonic intensity (b), i.e., the Maker fringe patterns, for the base glass and heat-treated samples as a function of rotation angle between linearly polarized incident lasers and samples in 40BaO–$40TiO_2$–$15SiO_2$–$5Al_2O_3$ glass. (a): the relation between incident lasers and samples.

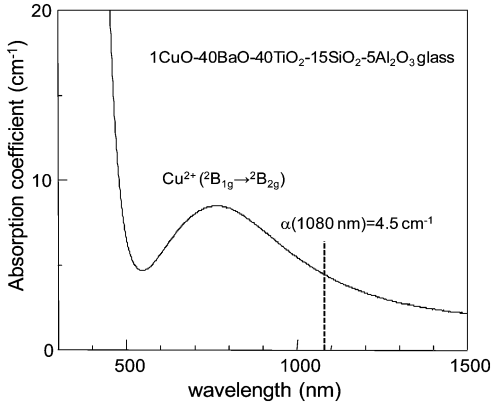

Fig. 6. Optical absorption spectrum at room temperature for 1CuO–40BaO–$40TiO_2$–$15SiO_2$–$5Al_2O_3$ glass.

ally to a tetragonal structure, i.e., the crystal structure in this region is pseudo-cubic. It is considered that the tetragonality in $BaTiO_3$ crystals present in the sample heat-treated at T_{p1} would be small, i.e., pseudo-cubic structure.

3.2 Patterning of $BaTiO_3$ crystal lines by laser irradiation

In the above experiments (Figs. 1 to 5), it was clarified that $BaTiO_3$ crystals are formed initially in the crystallization of 40BaO–$40TiO_2$–$15SiO_2$–$5Al_2O_3$ glass, and thus this glass would be a good candidate for the study of the laser pattering of $BaTiO_3$ crystals. The optical absorption spectrum at room temperature for 1CuO–40BaO–$40TiO_2$–$15SiO_2$–$5Al_2O_3$ glass (designated here as CuO-doped BTSA glass) is shown in **Fig. 6**. A broad and asymmetrical peak centered at ~800 nm is observed. It is well known that Cu^{2+} ions with the electronic configuration of $3d^9$ in glass give a strong and broad absorption peak at around 800 nm, and this peak is assigned to the $^2B_{1g} \rightarrow {}^2B_{2g}$ transition in Cu^{2+} ions in octahedral sites with strong tetragonal distortions.[34] The optical absorption coefficient of CuO-doped BTSA glass,

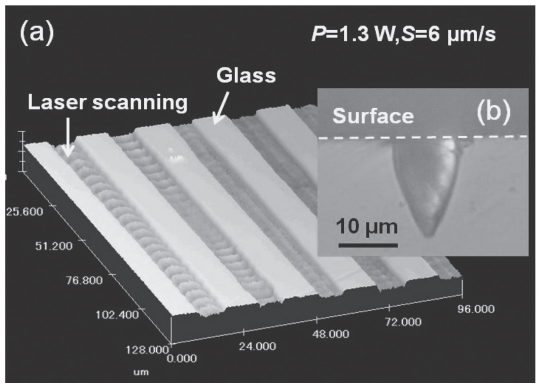

Fig. 7. CSLM photograph (a) for the sample obtained by cw Yb:YVO_4 laser irradiations ($\lambda = 1080$ nm) with a laser power of $P = 1.3$ W and a scanning speed of $S = 6$ μm/s and POM photograph (b) for the cross-section of the line in 1CuO–40BaO–$40TiO_2$–$15SiO_2$–$5Al_2O_3$ glass.

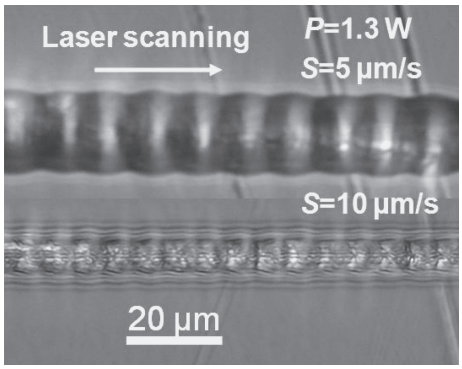

Fig. 8. POM photographs for the samples obtained by cw Yb:YVO_4 laser irradiations ($\lambda = 1080$ nm) with a laser power of $P = 1.3$ W and $S = 5$ and 10 μm/s in 1CuO–40BaO–$40TiO_2$–$15SiO_2$–$5Al_2O_3$ glass.

α, is found to be $\alpha = 4.5\,cm^{-1}$ at $\lambda = 1080$ nm. This absorption coefficient would be enough to induce structural modifications in BTSA glass by Yb:YVO_4 lasers,[19)–21),35)] although the fraction of nonradiative relaxation process for Cu^{2+} ions in BTSA glass is unclear.

We tried to pattern $BaTiO_3$ crystal lines with different laser irradiation conditions, i.e., different laser powers (P) and scanning speeds (S). As an example, the data obtained by cw Yb:YVO_4 laser irradiations ($\lambda = 1080$ nm) with a laser power of $P = 1.3$ W and $S = 6$ μm/s are shown in **Fig. 7**. The CSLM photograph [(a) in Fig. 7] indicates that laser irradiations induce clear structural changes at the glass surface. It is also seen that the morphology of the laser-irradiated surface is not smooth. The POM photograph [(b) in Fig. 7] for the cross-section of the line indicates that the width (W) of lines at the surface is $W = 11$ μm and the depth (D) is $D = 17$ μm. The shape of the cross-section shown in Fig. 7 is almost the same as that for ferroelectric $LiNbO_3$ crystals patterned by laser irradiations in 1CuO–$40Li_2O$–$32Nb_2O_5$–$28SiO_2$ glass.[27)] The region and shape of structural changes induced by laser irradiations would be related to the temperature profile (distribution) of laser-irradiated parts. The POM photographs for the samples obtained by laser irradiations with a laser power of $P = 1.3$ W and $S = 5$ and 10 μm/s are shown in **Fig. 8**. Structural changes are clearly induced along the laser scanning direction. The width of structure changed parts (lines) decreases with increasing laser scanning speed, i.e., $W = 20$ μm for $S = 5$ μm/s and $W = 5$ μm for $S = 10$ μm/s, and

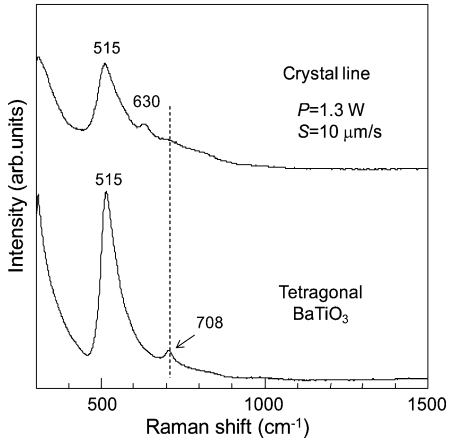

Fig. 9. Micro-Raman scattering spectrum at room temperature for the line patterned by lasers with $P = 1.3\,\mathrm{W}$ and scanning $S = 10\,\mu\mathrm{m/s}$ in $1\mathrm{CuO}$–$40\mathrm{BaO}$–$40\mathrm{TiO_2}$–$15\mathrm{SiO_2}$–$5\mathrm{Al_2O_3}$ glass.

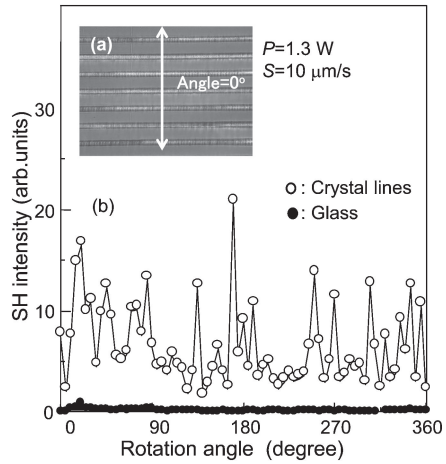

Fig. 10. Second harmonic intensity for the lines patterned by lasers with $P = 1.3\,\mathrm{W}$ and scanning $S = 10\,\mu\mathrm{m/s}$ in $1\mathrm{CuO}$–$40\mathrm{BaO}$–$40\mathrm{TiO_2}$–$15\mathrm{SiO_2}$–$5\mathrm{Al_2O_3}$ glass.

a periodic morphology change is observed clearly along the laser scanning direction. Even in other laser irradiation conditions, no success for the patterning of lines with a smooth surface has been achieved at this moment (in our study).

The micro-Raman scattering spectrum at room temperature for the line patterned by lasers with $P = 1.3\,\mathrm{W}$ and scanning $S = 10$ μm/s is shown in **Fig. 9**. The peaks are observed at 305, 515, and 630 $\mathrm{cm^{-1}}$, which are almost the same as those observed for the sample heat-treated at $T_{p1} = 826°\mathrm{C}$ for 5 h (Fig. 3). It should be pointed out that a broad peak is detected at $\sim 708\,\mathrm{cm^{-1}}$, although its intensity is very small. The peaks observed at 305 and $515\,\mathrm{cm^{-1}}$ demonstrate that at least $\mathrm{BaTiO_3}$ crystals are formed in the laser-irradiated parts. The SH intensity for the lines patterned by lasers with $P = 1.3\,\mathrm{W}$ and scanning $S = 10\,\mu\mathrm{m/s}$ is shown in **Fig. 10** as a function of the rotation angle between linearly polarized incident lasers and lines. In this experiment, the angles of 0 and 180° mean that an electric field of incident light is perpendicular to the crystal line growth direction (i.e., laser scanning direction). SHGs are clearly observed for the lines, indicating that $\mathrm{BaTiO_3}$ crystals being present in the laser-irradiated parts are nonlinear optical crystals. Furthermore, the results shown in Figs. 9 and 10 suggest that the crystal structure of $\mathrm{BaTiO_3}$ is not a perfect cubic, but has a small tetragonality.

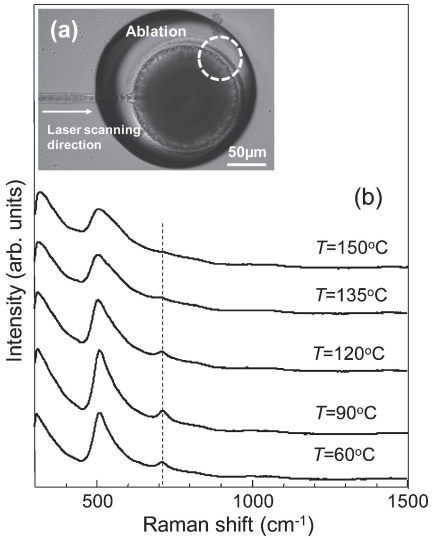

Fig. 11. POM photograph (a) for the sample with an ablation observed in the laser irradiations ($P = 1.3\,\mathrm{W}$ and $S = 10\,\mu\mathrm{m/s}$) in $1\mathrm{CuO}$–$40\mathrm{BaO}$–$40\mathrm{TiO_2}$–$15\mathrm{SiO_2}$–$5\mathrm{Al_2O_3}$ glass and Raman scattering spectra (b) measured at different temperatures for the part marked by a white circle in the POM photograph.

We tried cw $\mathrm{Yb{:}YVO_4}$ laser irradiations with different powers and scanning speeds for CuO-doped BTSA glass and also for other glasses such as $40\mathrm{BaO}$–$30\mathrm{TiO_2}$–$20\mathrm{SiO_2}$–$10\mathrm{Al_2O_3}$ and $35\mathrm{BaO}$–$45\mathrm{TiO_2}$–$15\mathrm{SiO_2}$–$5\mathrm{Al_2O_3}$ glasses. The results similar to the data shown in Figs. 9 and 10 are obtained. That is, the laser patterning of crystal lines consisting of tetragonal $\mathrm{BaTiO_3}$ has not been confirmed.

In the experiments of laser irradiations, accidentally there have been cases that structure change does not follow along laser scanning direction, but stops at a certain position. Such phenomena would be due to the presence of small dust at the glass surface or large surface roughness formed during the polishing of the glass surface. The stop of line growth provides ablation because laser energy is accumulated instantaneously in a limited region. The POM photograph for such an ablation observed in the laser irradiations ($P = 1.3\,\mathrm{W}$ and $S = 10\,\mu\mathrm{m/s}$) in CuO-doped BTSA glass is shown in **Fig. 11**(a). We checked the structure change in this ablation region from micro-Raman scattering spectrum measurements, and the data are shown in Fig. 11(b). As a result, it was found that the certain region, which is marked as a white circle in the POM photograph in Fig. 11(a), consists of tetragonal $\mathrm{BaTiO_3}$ crystals, because Raman-active bands being typical for tetragonal $\mathrm{BaTiO_3}$, i.e., 305, 515, and $708\,\mathrm{cm^{-1}}$, are detected. In order to confirm more clearly the formation of tetragonal $\mathrm{BaTiO_3}$ crystals, the temperature dependence of Raman scattering spectrum was measured, and the results are shown in Fig. 11(b). It is seen that the intensity of three peaks decreases with increasing temperature. In particular, the intensity of the peak at $708\,\mathrm{cm^{-1}}$ is extremely small at 135°C and almost disappears at 150°C. It is well known that the phase transition temperature from tetragonal to cubic in $\mathrm{BaTiO_3}$ crystals is around 135°C.[30),33)] Consequently, the data shown in Fig. 11 demonstrate that tetragonal $\mathrm{BaTiO_3}$ crystals are formed in the ablation region produced by laser irradiations. At this moment, information on the morphology and size of $\mathrm{BaTiO_3}$ crystals formed by laser irradiations has not been obtained. Further studies such as high resolution transmission electron microscope observations would be necessary.

As shown in Table 1, various studies on the synthesis of $BaTiO_3$ crystals through the crystallization of glasses have been reported, and it has been recognized that the crystallization of tetragonal $BaTiO_3$ as an initial crystalline phase, i.e., the crystallization at low temperatures, is difficult. For instance, Kusumoto et al.[8] reported that $BaTiO_3$ crystals formed in $50BaO–20TiO_2–30B_2O_3$ glass are cubic in the low temperature annealing (700°C), while apparently tetragonal in the high temperature annealing (800°C or above). Narazaki et al.[12] examined the crystallization behavior of $BaTiO_3$ in $15BaO–15TiO_2–70TeO_2$ glass[7] and $BaTiO_3$ crystals formed exhibit SHGs, although the structure is closer to cubic than tetragonal according to XRD measurements. The present study also proposes that the crystal growth rate of $BaTiO_3$ in glasses is not so high, providing nano-scaled crystals (i.e., below 100 nm) with a pseudo-cubic structure and that basically crystallization at high temperature is required in order to synthesize tetragonal $BaTiO_3$ crystals with a large size. The crystallization of glass proceeds through two steps of crystal nucleation and growth, and atomic rearrangements are taking place. In the case of the crystallization of $BaTiO_3$ in $40BaO–40TiO_2–15SiO_2–5Al_2O_3$ glass, the diffusion of Ba^{2+}, Ti^{4+}, and O^{2-} ions or structural units such as TiO_n polyhedra is required. It is obvious that the glass network constructed by SiO_2 and Al_2O_3 prevents their long-range diffusions, consequently depressing the large crystal growth of $BaTiO_3$. So far, ferroelectric crystals with high orientations such as $LiNbO_3$, $NaNbO_3$ and β'-$Gd_2(MoO_4)_3$ have been patterned successfully by designing glass composition and laser irradiation conditions.[19)–23),27),36),37)] For the laser patterning of homogeneous lines with tetragonal $BaTiO_3$ single crystals, further study, in particular on the glass system and composition, would be required.

4. Conclusion

The formation behavior and characterization of $BaTiO_3$ crystals in $40BaO–40TiO_2–15SiO_2–5Al_2O_3$ glass were examined from X-ray diffraction analyses, Raman scattering spectrum, second harmonic generation (SHG), and polarization measurements. The structure of $BaTiO_3$ formed initially was suggested to be pseudo-cubic (small tetragonality), and perovskite-type ferroelectric $BaTiO_3$ crystals were formed in the heat-treatments at high temperatures of ~930°C. The lines consisting of $BaTiO_3$ crystals were patterned at the surface of CuO-doped glass by irradiations of continuous-wave Yb:YVO_4 lasers with a wavelength of 1080 nm. It was confirmed that $BaTiO_3$ being present in the laser-irradiated parts exhibits SHGs and, in particular, $BaTiO_3$ formed in the laser ablation region has a Curie temperature of ~135°C.

Acknowledgements This work was supported from the Grant-in-Aid for Scientific Research from the Ministry of Education, Science, Sports, Culture and Technology, Japan (No. 23246114) and by Program for High Reliable Materials Design and Manufacturing in Nagaoka University of Technology.

References

1) A. Herczog, *J. Am. Ceram. Soc.*, **47**, 107–115 (1964).
2) T. Kokubo, S. Sakka and M. Tashiro, *J. Ceram. Soc. Japan*, **74**, 517-522 (1966).
3) T. Kokubo, C. T. Kung and M. Tashiro, *J. Ceram. Soc. Japan*, **77**, 529–533 (1966).
4) M. M. Layton and A. Herczog, *Glass Technol.*, **10**, 50–53 (1969).
5) N. F. Borrelli and M. M. Layton, *J. Non-Cryst. Solids*, **6**, 197–212 (1971).
6) A. Bhargava, J. E. Shelby and R. L. Snyder, *J. Non-Cryst. Solids*, **102**, 136–142 (1988).
7) T. Komatsu, H. Tawarayama and K. Matusita, *J. Ceram. Soc. Japan*, **101**, 48–52 (1993).
8) K. Kusumoto, T. Sekiya and Y. Murase, *Mater. Res. Bull.*, **28**, 461–467 (1993).
9) M. Todorovic, Lj. Radonjic and J. Dumic, *Key Eng. Mater.*, **132–136**, 193–196 (1997).
10) C. A. Randall, D. E. McCauley and D. P. Cann, *Ferroelectrics*, **206–207**, 325–335 (1998).
11) D. McCauley, R. E. Newnham and C. A. Randall, *J. Am. Ceram. Soc.*, **81**, 979–987 (1998).
12) A. Narazaki, K. Tanaka and K. Hirao, *J. Mater. Res.*, **14**, 3640–3646 (1999).
13) Y. Yonesaki, K. Miura, R. Araki, K. Fujita and K. Hirao, *J. Non-Cryst. Solids*, **351**, 885–892 (2005).
14) E. K. Abdel-Khalek, E. A. Mohamed, S. M. Salem, F. M. Ebrahim and I. Kashif, *Mater. Chem. Phys.*, **133**, 69–77 (2012).
15) K. Kakegawa and J. Takahashi, *J. Am. Ceram. Soc.*, **87**, 1602–1605 (2004).
16) P. V. Divya and V. Kumar, *J. Am. Ceram. Soc.*, **90**, 472–476 (2007).
17) E. P. Gorzkowski, M. J. Pan, B. A. Bender and C. C. M. Wu, *J. Am. Ceram. Soc.*, **91**, 1065–1069 (2008).
18) A. K. Yadav, C. Gautam and P. Singh, *New J. Glass Ceram.*, **2**, 126–131 (2012).
19) T. Komatsu, R. Ihara, T. Honma, Y. Benino, R. Sato, H. G. Kim and T. Fujiwara, *J. Am. Ceram. Soc.*, **90**, 699–705 (2007).
20) T. Komatsu and T. Honma, *IEEE J. Sel. Top. Quantum Electron.*, **14**, 1289–1297 (2008).
21) T. Honma, *J. Ceram. Soc. Japan*, **118**, 71–76 (2010).
22) T. Komatsu, F. Suzuki, K. Ogawa and T. Honma, *Transactions on GIGAKU*, **1**, 01017 (2012).
23) T. Honma, Y. Benino, T. Fujiwara and T. Komatsu, *Appl. Phys. Lett.*, **88**, 231105 (2006).
24) T. Honma, K. Koshiba, Y. Benino and T. Komatsu, *Opt. Mater.*, **31**, 315–319 (2008).
25) T. Honma, T. Komatsu, D. Zhao and H. Jain, *IOP Conf. Series: Mater. Sci. Eng.*, **1**, 012006 (2009).
26) T. Honma and T. Komatsu, *Opt. Express*, **18**, 8019–8024 (2010).
27) T. Komatsu, K. Koshiba and T. Honma, *J. Solid State Chem.*, **184**, 411–418 (2011).
28) T. Oikawa, T. Honma and T. Komatsu, *Cryst. Res. Technol.*, **43**, 1253–1257 (2008).
29) L. Aleksandrov, T. Komatsu, R. Iordanova and Y. Dimitriev, *Opt. Mater.*, **33**, 839–845 (2011).
30) B. D. Begg, K. S. Finnie and E. R. Vance, *J. Am. Ceram. Soc.*, **79**, 2666–2672 (1996).
31) T. Noma, S. Wada, M. Yano and T. Suzuki, *J. Appl. Phys.*, **80**, 5223–5233 (1996).
32) Z. Yao, H. Liu, Y. Liu, Z. Wu, Z. Shen, Y. Liu and M. Cao, *Mater. Chem. Phys.*, **109**, 475–481 (2008).
33) K. Suzuki and K. Kijima, *J. Alloys Compd.*, **419**, 234–242 (2006).
34) R. P. S. Chakradhar, B. Yasoda, J. L. Rao and N. O. Gopal, *J. Non-Cryst. Solids*, **352**, 3864–3871 (2006).
35) K. Koshiba, T. Honma, Y. Benino and T. Komatsu, *Appl. Phys., A Mater. Sci. Process.*, **89**, 981–986 (2007).
36) Y. Tsukada, T. Honma and T. Komatsu, *Appl. Phys. Lett.*, **94**, 059901 (2009).
37) K. Kioka, T. Honma, K. O-ishi, S. Leibstein, N. Da, L. Wondraczek and T. Komatsu, *J. Non-Cryst. Solids*, **358**, 1523–1529 (2012).